ARTICLE
Journal of Cellular Biochemistry 108:96–105 (2009)

Journal of Cellular Biochemistry

Synchrotron X-Ray Imaging Reveals a Correlation of Tumor Copper Speciation With Clioquinol's Anticancer Activity

Raul A. Barrea,[1*] Di Chen,[2] Thomas C. Irving,[1] and Q. Ping Dou[2]

[1] *Biophysics Collaborative Access Team (BioCAT), CSRRI and Dept of Biological Chemical, and Physical Sciences, Illinois Institute of Technology, Chicago, Illinois, 60616*

[2] *The Prevention Program, Barbara Ann Karmanos Cancer Institute, and Department of Pathology, School of Medicine, Wayne State University, Detroit, Michigan 48201-2013*

ABSTRACT

Tumor development and metastasis depend on angiogenesis that requires certain growth factors, proteases, and the trace element copper (Cu). Recent studies suggest that Cu could be used as a novel target for cancer therapies. Clioquinol (CQ), an antibiotic that is able to form stable complexes with Cu or zinc (Zn), has shown proteasome-inhibitory, androgen receptor-suppressing, apoptosis-inducing, and antitumor activities in human cancer cells and xenografts. The mechanisms underlying the interaction of CQ with cellular Cu, the alteration of the Cu/Zn ratio and the antitumor role of CQ in vivo have not been fully elucidated. We report here that Cu accumulates in tumor tissue and that the Cu/Zn balances in tumor, but not normal, tissue change significantly after the treatment with CQ. Cu speciation analysis showed that the Cu(I) species is predominant in both normal and tumor tissues and that Cu(II) content was significantly increased in tumor, but not normal tissue after CQ treatment. Our findings indicate that CQ can interact with cellular Cu in vivo, dysregulates the Cu/Zn balance and is able to convert Cu(I) to Cu(II) in tumor tissue. This conversion of Cu(I) to Cu(II) may be associated with CQ-induced proteasome inhibition and growth suppression in the human prostate tumor xenografts. J. Cell. Biochem. 108: 96–105, 2009.

KEY WORDS: CLIOQUINOL; COPPER; ANTICANCER DRUGS; SYNCHROTRON X-RAY IMAGING

In industrialized countries, cancer of the prostate is one of the most frequently diagnosed forms and is the second leading cause of death in men [Jemal et al., 2006]. Development and metastasis of human prostate and other cancers depend on angiogenesis that requires certain growth factors, proteases, and the trace element copper (Cu) [Brem, 1999; Brewer, 2001; Theophanides and Anastassopoulou, 2002; Daniel et al., 2004]. The notion that Cu could be used as a novel selective target for cancer therapies has been supported by the following lines of evidence. (i) High serum or tissue levels of Cu have been found in many types of human cancers, including prostate, breast, colon, lung, and brain [Habib et al., 1980; Rizk and Sky-Peck, 1984; Turecky et al., 1984; Huang et al., 1999; Nayak et al., 2003]. (ii) In normal organs (e.g., liver) of human and mammals, there are no known harmful effects observed when the bioavailability of Cu is decreased up to 80% from baseline [Goodman et al., 2004]. (iii) Therapies using the strong Cu chelator tetrathiomolybdate (TM) are well tolerated and Cu elimination can stabilize advanced kidney cancer [Brewer et al., 2000], demonstrating the clinical feasibility of this approach.

While the exact role of Cu in the tumor angiogenesis process is unclear, recent X-ray fluorescence microscopy studies revealed that there is a large-scale relocalization and extra cellular translocation of cellular Cu during angiogenesis [Finney et al., 2007]. These findings suggest that relocalization of Cu during angiogenesis may be caused by the movement of Cu chaperone proteins. If so, a Cu chelator could interfere with the tumor angiogenesis process by competing against the Cu chaperone proteins, therefore inhibiting the Cu-dependent functions of these regulatory proteins and, hence, angiogenesis.

Cu homeostasis in human is tightly regulated by several different systems. The major source of Cu is from food and drinking. After

Grant sponsor: Karmanos Cancer Institute of Wayne State University, Department of Defense Breast Cancer Research; Grant numbers: W81XWH-04-1-0688, DAMD17-03-1-0175; Grant sponsor: National Cancer Institute; Grant number: CA112625; Grant sponsor: National Center for Research Resources; Grant number: RR08630; Grant sponsor: U.S. Department of Energy, Basic Energy Science, Office of Energy Research; Grant number: W-31-109-Eng-38.

*Correspondence to: Prof. Raul A. Barrea, 9700 S Cass Ave, BioCAT/Bldg 435, Argonne, IL 60439.
E-mail: rbarrea@gmail.com

Received 26 January 2009; Accepted 5 May 2009 • DOI 10.1002/jcb.22231 • © 2009 Wiley-Liss, Inc.
Published online 15 June 2009 in Wiley InterScience (www.interscience.wiley.com).

absorption from the gastrointestinal system, Cu in serum is carried mainly by the Cu carrier ceruloplasmin. Cu uptake by cells is through a Cu transporter 1 (Ctr1) in the cell membrane. Most of the cellular Cu is found in the form of Cu(I). After being imported into a cell by Ctr1, Cu(I) binds to Cu chaperone proteins, such as apo-ATX1 and diffuses throughout the cytoplasm, remaining as Cu(I) in an all-sulfur coordination environment along its pathways [Pufahl et al., 1997]. Microspectroscopy studies of intra-cellular Cu showed that Cu(I) is the predominant Cu species in cultured fibroblast 3T3 cells (although the presence of Cu(II) species could not be completely excluded) [Yang et al., 2005]. Studies of Cu K edge by X-ray absorption near edge spectroscopy (XANES) also revealed a significant colocalization of Cu and sulfur (S), indicating that Cu might be coordinated with sulfur donor ligands in a linear or trigonal geometry. Since the ''free'' pools of Cu are far less than a single atom per cell [Rae et al., 1999], it is believed that most of the cellular Cu is bound by various Cu chaperones that first receive Cu and then deliver it to specific locations [Macreadie, 2008]. This hypothesis is also supported by our previous findings in which (i) Cu ion could potently inhibit the activity of a purified 20S proteasome but could not do so when used in intact cells [Chen et al., 2007], and (ii) treatment of Cu-enriched human prostate cancer cells with the Cu-binding antibiotic Clioquinol (CQ) could inhibit proteasome activity and induce apoptotic cell death [Chen et al., 2007]. In one possible mechanism, it is assumed that within a cell, CQ could competently take over Cu from Cu chaperon proteins and make it possible for the Cu to interact with the proteasome, resulting in inhibition of proteasome activity and induction of apoptosis. However, direct evidence supporting such a CQ-cellular Cu interaction is needed.

Zinc (Zn) is one of the essential elements for the human body. Zn has been shown to play an important role in the structure and function of many enzymes, including oxidoreductase, alcohol dehydrogenase (ADH), and matrix metalloproteinases (MMPs) [Vallee and Auld, 1990]. The human prostate normally accumulates 2–5 times more Zn than any other tissues and 35% of that Zn exists as ''free'' or loosely bound. It is well known that the Zn content in prostate cancer tissue is at a lower level than in normal tissue, mainly because premalignant and malignant cells are not capable of accumulating high Zn levels [Habib et al., 1979; Costello and Franklin, 1998]. An early study using X-ray fluorescence microscopy on human prostate showed a higher local Zn content in normal epithelial cells compared with adenocarcinoma [Habib et al., 1979]. Accumulation of Zn in the stroma of tumor tissues was also observed [Habib et al., 1979]. Normal tissue showed a larger dispersion of Zn values probably due to ''free'' Zn content fluctuation [Ide-Ektessabi et al., 2002]. In tumor tissues of patients with prostate and ovarian cancers, increased Cu levels and decreased Zn levels were observed [Guntupalli et al., 2007]. The mean Cu/Zn ratio in the ovarian tumor tissues of the patients was 60% higher than that in the benign tissues [Lightman et al., 1986]. This increase is even more dramatic in prostate tumor tissue where the ratio was 0.367 as compared to a normal ratio of 0.0063. This 60 times increased ratio in the tumor tissue is due to an eightfold increase in Cu content and a sevenfold decrease in Zn content [Guntupalli et al., 2007]. Therefore, the Cu/Zn balance is altered in tumors because tumor cells tend to accumulate more Cu and at the same time fail to accumulate Zn. The mechanisms behind these changes are not fully understood.

CQ is a quinol that selectively binds with both Cu(II) and Zn(II), forming very stable complexes [Di Vaira et al., 2004]. It has been reported that the CQ affinity for Cu(II) is higher than for Zn(II) [Ferrada et al., 2007], and it has also been suggested that CQ may form complexes with Cu(II), even in the presence of competing ions and beta-amyloid plaques or huntingtin. Therefore, CQ–Cu binding is tighter than for beta-amyloid-Cu [Puig and Thiele, 2002; Ferrada et al., 2007]. CQ is a membrane-permeable compound [Nitzan et al., 2003]. Pharmacokinetic studies of CQ have shown that after a single oral dose of CQ, the peak concentration appears around 4 h after ingestion. After absorption, CQ is metabolized to sulfates and glucoronides. CQ is excreted out of a human body as free CQ and as glucuronide and sulfate metabolites [Degen et al., 1979a,b]. In the study of oral CQ for the treatment of Alzheimer's disease, the serum levels of CQ are in a range of 13–25 μM [Ritchie et al., 2003], which are within the range required to exert an antitumor effect in culture. CQ has been used in clinical treatments as antibiotic for diarrhea and skin infections. Although it was withdrawn from the market due to a potential association with toxic effects causing subacute myelo-optic neuropathy, these conclusions were not supported by later epidemiologic studies. Recent studies show that CQ has the potential for the treatment of Alzheimer and Huntington diseases [Ritchie et al., 2004; Nguyen et al., 2005].

Our most recent study using human prostate cancer cultures and xenografts suggests that CQ, after forming a CQ–Cu(II) complex, has proteasome-inhibitory activity, represses androgen receptor expression and induces apoptotic cell death [Chen et al., 2007]. The mechanism responsible for the CQ-mediated antitumor activity has not been fully elucidated. The main outstanding questions are: (i) Does CQ interact with extra-cellular Cu during angiogenesis, forming a CQ–Cu complex inhibiting the formation of new blood vessels and therefore tumor growth [Chen et al., 2007]? (ii) Does CQ interact with extra-cellular Cu and then transport it into the cell? (iii) Does CQ act as a chelator of intra-cellular Cu in tumor cells? If so, (iv) does the formed CQ–Cu complex have any biological activity?

To address at least some of these questions and to further understand the molecular mechanism of CQ-mediated antitumor activity, we performed an animal experiment in which human prostate tumor xenografts were treated with CQ or the control vehicle, followed by measurements of elemental mapping and chemical status of Cu in both tumor and normal tissues collected from the same mice. Our results strongly suggest that CQ interacts with cellular Cu in tumors and forms an anticancer CQ–Cu(II) complex in vivo.

RESULTS

VARIATIONS OF Cu AND Zn CONTENT IN NORMAL AND TUMOR TISSUES

It has been shown that CQ binds to Cu forming a CQ–Cu(II) complex in solution and that CQ is capable of inhibiting proteasome activity,

suppress androgen receptor expression, induce apoptosis, and inhibit angiogenesis in human prostate tumor xenografts [Chen et al., 2007]. To further investigate whether CQ could bind to the elevated Cu content in tumor tissue (which is low in normal tissue), forming a tumor-specific CQ–Cu complex in vivo, we performed an animal experiment in which human prostate tumor xenografts were treated with either CQ or control vehicle (CON). Tumor samples were obtained from the human prostate tumor C4-2B xenografts grown in nude mice, while the normal tissues were from the sites adjacent to the xenografts form the same mice. Samples were analyzed by scanning X-ray florescence microscopy (XFM) and X-ray absorption spectroscopy measurements to obtain elemental maps of Cu and Zn in both normal control (NCON) and CQ-treated normal (NCQ) tissues and untreated tumor (TMR) and CQ-treated tumor (TCQ) tissues as shown in Figure 1. The elemental concentrations in $\mu g/cm^2$ are represented in color code. It is clear that the Cu and Zn distributions are not homogeneous in these samples. The Cu accumulation observed in control tissue NCON (0.0001–0.0100 $\mu g/cm^2$) is similar to that found in NIH 3T3 cells that were cultured in basal medium [Yang et al., 2005]. Zn content was also found to be in a similar range as in fibroblast cells.

We observed a significant increased Cu content in the untreated tumor (TMR) sample compared with the control tissue sample (NCON, Fig. 1). This extra Cu may be located in intracellular compartments of tumor cells and in new blood vessels being formed. In addition, increased Zn content was also found (Fig. 1). Although Zn was expected to be decreased in tumor tissue, the observed increase of Zn in the tumor may be due to the fact that tumor sample was from human prostate tumor cells while normal sample was from mouse flank tissue, since the prostate gland actually contains a higher level of Zn than any other gland or tissue [Zaichick et al., 1997; Costello and Franklin, 1998].

No significant variations of the Cu and Zn content in normal tissue was found after CQ treatment (NCQ). Although there appears to be a slight increase in normal tissue Zn levels after CQ treatment in the data shown in Figure 1, analysis of multiple areas of the normal tissue samples indicate that CQ treatment does not increase Zn content (see Fig. 2). Tumor tissue, however, shows a significant decrease in both Cu and Zn content after CQ treatment (TCQ). These results suggest an active interaction of CQ with the extra endogenous cellular Cu available and/or the exogenous cellular Cu located in the newly formed blood vessels in the tumor, since it is possible that CQ could get into the bloodstream and interact with the metal in the blood, which could lead to decreased levels of Cu and Zn in the tumor tissues. It should be noted that any CQ–Cu interactions will not mask the detection of Cu atoms in the sample by XFM. Therefore, the decrease of Cu content must be directly associated with an actual variation of total Cu in the sample. Previously it was found that CQ was able to bind to both Cu and Zn [Di Vaira et al., 2004]. Whether decreased Zn content in CQ-treated tumor is due to the same mechanism remains to be determined.

Cu/Zn RATIO IN NORMAL AND TUMOR TISSUES AFTER CQ TREATMENT

Due to the non-homogeneous distribution of the elements on the different tissue sections, visual comparison of the elemental maps may miss real differences among them, while pixel-by-pixel

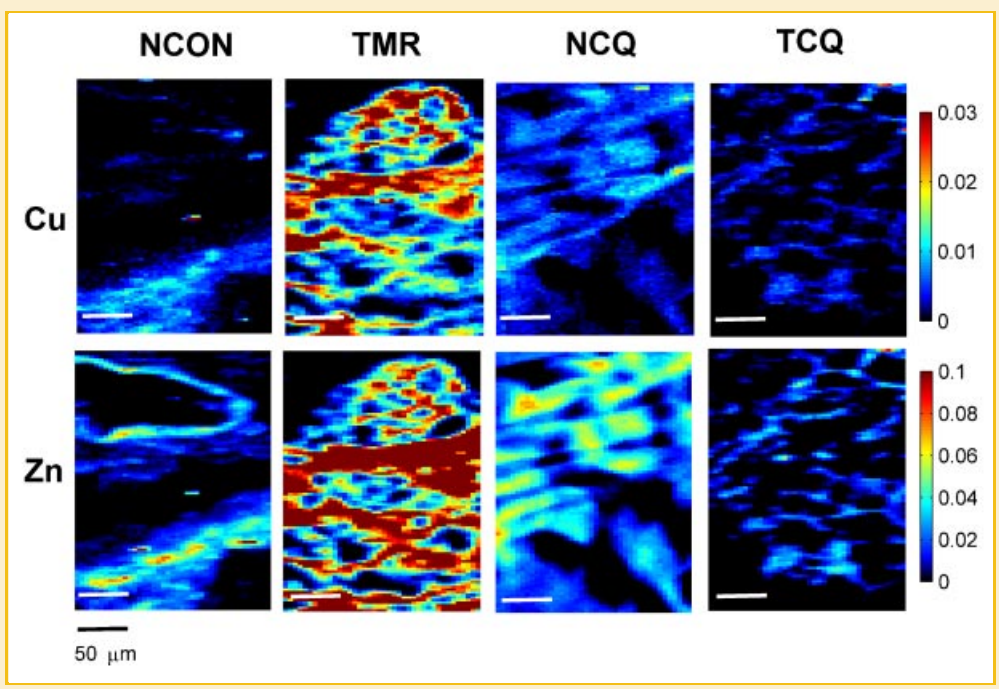

Fig. 1. Imaging of normal and tumor tissue Cu and Zn distributions by XFM. NCON, normal tissue from control group; TMR, untreated tumor tissue; NCQ, normal tissue from CQ-treated group; TCQ, tumor tissue from CQ-treated group. The calibrated elemental concentrations in $\mu g/cm^2$ are represented by the color code; the same scale is used for both elements.

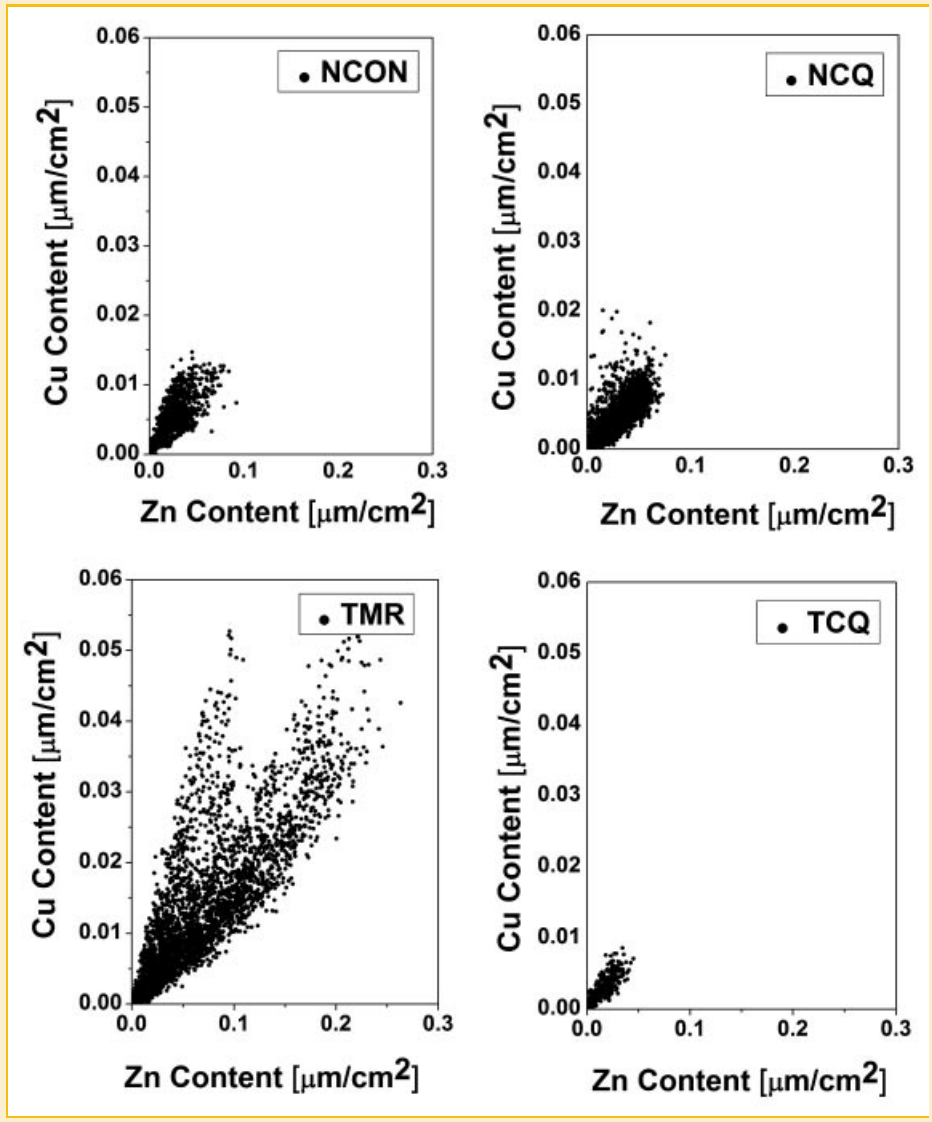

Fig. 2. Cu content per pixel from the imaging maps is plotted against its corresponding Zn content to observe their correlation in normal and tumor tissue. It is clearly seen that CQ treatment (NCQ) did not substantially modify the Cu–Zn correlation in normal tissue (NCON). In tumor (TMR), the Cu–Zn correlation is different from the normal correlations showing two regions of clustered data. After CQ treatment, tumor tissue (TCQ) shows a substantial reduction in Cu content but the Cu–Zn correlation resembles the correlation observed in normal tissue.

analysis performed on images from normal and tumor tissue could show significant differences.

Plots of Cu content as a function of Zn content for NCON and CQ-treated normal (NCQ) samples (Fig. 2) are not distinguishable, indicating that CQ treatment does not modify the relationship of Cu to Zn content in normal tissue. One can look at the relationship of Cu to Zn in another way that is independent of the absolute Zn or Cu contents by examining the Cu/Zn ratio. This can reduce bias due to inhomogeneities in tissue thickness and other sources of variability. The histogram of frequencies of Cu/Zn ratio (NCON and NCQ in Fig. 3) shows a unimodal distribution with a maximum between 0.12 and 0.18 for the Cu/Zn ratio. In sharp contrast, plots of Cu content as a function of Zn content for tumor sample (TMR, Fig. 2) present a different pattern compared to those observed in normal tissues (NCON and NCQ in Fig. 2), The data appears to be clustered around two relationships, one with a steeper slope than the other. Consistent with this observation, the Cu/Zn histogram clearly shows a bimodal distribution (TMR, Fig. 3). One group of values could be associated with normal cells since their Cu/Zn distribution is similar to that observed in normal cells (NCON and NCQ, Fig. 3). The other group of values presents a peak at a higher value and with a wider distribution. This group could be identified with tumor cells that show large increase of Cu content (up to five times increase in some areas) with small increase of Zn content (only a factor of two increase) compared to normal cells. This might be associated with an area of the tumor under invasion, since additional accumulation of Cu is required for angiogenesis [Brem, 1999; Brewer, 2001; Theophanides and Anastassopoulou, 2002; Daniel et al., 2004].

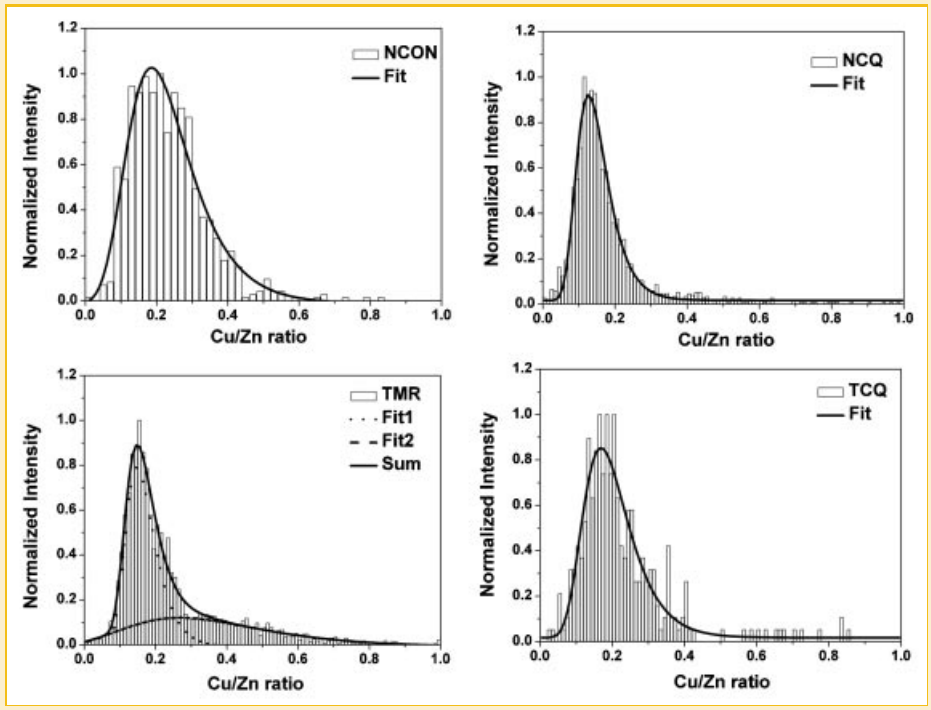

Fig. 3. Histogram of frequencies for the Cu/Zn ratio. Normal control and CQ-treated normal tissue (NCON and NCQ) show a unimodal distribution indicating CQ treatment did not alter the Cu/Zn correlations. Tumor tissue (TMR) shows a bimodal distribution. After CQ treatment, tumor tissue shows a unimodal distribution similar to that of normal control and CQ-treated normal samples. A lognormal distribution function was assumed to fit the Cu/Zn distribution curves.

The relationship between Cu content and Zn content in CQ-treated tumor (TCQ, Fig. 2), extend over a smaller range as compared to normal samples (NCON and NCQ, Fig. 2) indicating that the total content for both metals is lower. The histogram of frequencies of Cu/Zn ratio of CQ-treated tumor (TCQ, Fig. 3) shows a unimodal distribution similar to that of normal tissue (NCON and NCQ, Fig. 3). These results suggest that there is an interaction of CQ with intracellular and extra cellular Cu (and possibly with cellular Zn) that modifies the Cu/Zn balance found in tumors. This could be due to induction of cell death in the second group of tumor cells and/or converting the second to the first group of cells.

Cu(I) IS PREDOMINANT IN NORMAL AND TUMOR TISSUES

XANES at the Cu K absorption edge has been measured on Cu standards and tissue samples to identify the presence of different Cu species. Cu(I) and Cu(II) species show specific XANES spectral features that allow unambiguous identification of each oxidation state and its coordination environment [Kau et al., 1987; Yang et al., 2005].

All tissue samples show similar features that mainly correspond to Cu(I) oxidation state. The strong peak at 8,983 eV clearly indicates the presence of Cu(I) species in all tissue samples (indicated by line b, Fig. 4). These spectra seem to fit well with a trigonal arrangement with all sulfur ligands. The weak pre-edge peak at 8,978 eV (indicated line a, Fig. 4), which would be indicative of the Cu(II) species, is not clearly seen, although it is difficult to conclude that the peak is completely absent because of the low signal to noise ratio. Thus, the presence of low concentrations of Cu(II) species in some localized areas cannot be completely excluded.

CQ TREATMENT RESULTS IN A SIGNIFICANT INCREASING Cu(II) CONTENT IN TUMOR TISSUE

Figure 5 shows total Cu, Cu(I), and Cu(II) maps for each measured sample. It should be noted that unlike the data shown in Figure 1 that were normalized by using NIST standards, the results in Figure 5 were not normalized and while they thus do not represent accurate absolute amounts, they serve to show the relative amounts of Cu(I) and Cu(II) content in the samples. Normal tissue maps (Fig. 5) show a predominantly Cu(I) content with a Cu(II)/Cu(I) ratio of 0.1 in some scanned areas (data not shown). This suggests the predominance of Cu(I) species in normal tissue in accordance with previous results of intracellular XANES [Rae et al., 1999]. CQ treatment, however, shows no effect on the Cu speciation in normal cells (NCQ, Fig. 5), further supporting the argument that CQ does not interact with Cu in normal tissue.

In general, untreated tumor tissue (TMR) presents predominantly Cu(I) content, although in some locations the observed Cu(II)/Cu(I) ratio can be up to 0.2 (TMR, Fig. 5). This suggests that tumor progression involves not only additional Cu accumulation but also Cu oxidation as well.

In the case of CQ-treated tumor tissue (TCQ) there are spots where the Cu(II)/Cu(I) ratio is as high as 0.5 (Fig. 5). This increase in Cu(II) content, although localized and qualitative, suggests that CQ has formed a complex with cellular Cu in treated tumor. These data

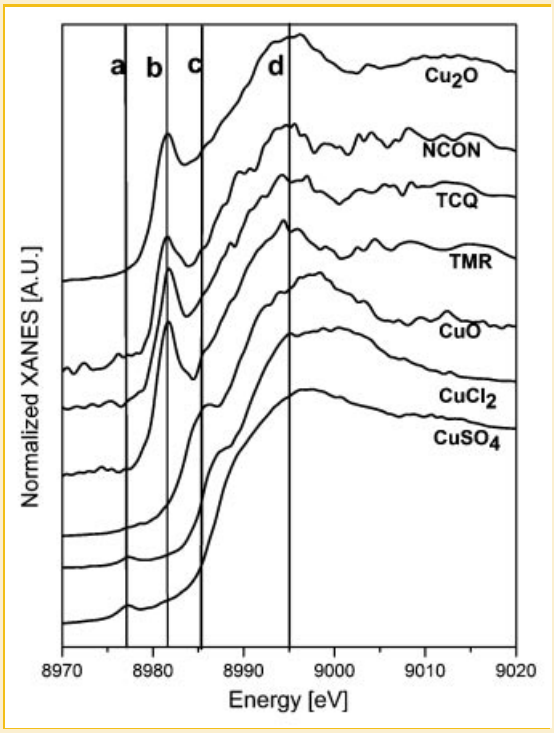

Fig. 4. XANES of Cu standards ($Cu_2(I)O$; Cu(II)O; $Cu(II)Cl_2$; $Cu(II)SO_4$) measured at the Cu K edge were used as reference for Cu(I) and Cu(II) status. XANES spectra from three tissue samples: NCON, TMR, and TCQ are also shown. XANES spectra were acquired with an unfocused X-ray beam. XANES curves were shifted vertically to ease visualization of the curve's features. See Materials and Methods Section for details.

consistently support the idea that CQ not only interacts with cellular Cu in vivo and dysregulates the Cu/Zn balance but also is able to increase the Cu(II)/Cu(I) ratio in tumor tissue. This suggests three possible mechanisms for CQ–Cu interaction in tumor cells: direct conversion of Cu(I) in Cu(II); CQ reacts with exogenous Cu(II) then transport it to the cell; or that CQ reacts with the available Cu(II) in tumor (the later alone would not explain the increase in Cu(II)/Cu(I) ratio in tumor tissue).

DISCUSSION

We have previously found several organic Cu complexes that selectively inhibit proteasome activity and induce apoptosis in tumor but not in normal cells [Daniel et al., 2004]. We have also shown that CQ forms a complex with Cu that can inhibit the proteasome activity and cell proliferation and induce apoptosis in breast and prostate cancer cells and/or xenografts in nude mice [Chen et al., 2005; Daniel et al., 2005]. We and others have found that Zn also has a potential to inhibit the proteasome [Amici et al., 2002; Kim et al., 2004; Milacic et al., 2008]. However, the mechanism by which CQ interacts with metals, especially Cu, in vivo to present its antitumor activity has not yet been revealed. In the current study, we hypothesized that CQ interacts with Cu and dysregulates the Cu/Zn balance in tumor cells. To test this hypothesis, CQ-treated human prostate tumor xenografts along with NCON were used for measurements of elemental mapping and chemical status of Cu.

We first demonstrated that CQ treatment causes a change in Cu and Zn content in tumor but not normal tissue (Figs. 1 and 2). After CQ treatment the levels of Cu and Zn decreases dramatically in tumor tissue but no such decrease is found in normal tissues (Figs. 1 and 2), suggesting that CQ could target Cu and Zn selectively in tumor but not normal tissue. Interestingly, treatment with CQ resulted in a reduction of Cu content in tumor tissue to levels similar to that found in normal tissue (Figs. 1 and 2). This decreased Cu content after CQ treatment may be associated with (i) a lower demand for Cu by the tumor (because of significant tumor suppression and apoptosis after 15-day treatment with CQ) and/or (ii) less Cu accumulation in the tumor (because of a significant decreased blood vessel formation due to CQ treatment).

We then analyzed the Cu/Zn ratio in normal and tumor tissues from control- and CQ-treated animals. Inutsuka and Araki [1978] compared Cu/Zn ratio in serum between a normal group and patients with digestive carcinomas and revealed that the Cu/Zn ratio was 0.81 ± 0.17 in the normal group and 1.49 ± 0.50 in the cancer patients. In the same studies it was found that Cu/Zn ratio further increased to 2.02 ± 0.48 in advanced digestive carcinomas with liver metastasis [Inutsuka and Araki, 1978]. These findings demonstrated that these increases in the Cu/Zn ratio were not only associated with malignant diseases but also associated with stages of cancers. The Cu/Zn ratio was also found increased in breast cancer patients (1.91 vs. 0.86 in the normal) but not increased in patients with benign breast diseases [Gupta et al., 1991]. The mechanism responsible for increased Cu/Zn ratios in cancer patients needs to be fully elucidated but a proposed mechanism for these alterations is associated with angiogenesis in malignant diseases [Raju et al., 1982; Parke et al., 1988]. The observed bimodal distribution of Cu/Zn ratio frequencies from the untreated tumor sample (TMR, Fig. 3) could be associated with tumor cells that show large increase of Cu content and low Zn content. From the CQ-treated tumor sample (TCQ, Fig. 3) the observed Cu/Zn distribution resembles the distribution found in NCON sample (NCON, Fig 3). The Cu/Zn balance in normal tissue was not modified after CQ treatment (comparison between NCON and NCQ samples, Fig. 3). In tumor, CQ interaction with intra-cellular and extra cellular Cu (and possibly with cellular Zn as well) modified significantly the Cu/Zn balance to levels similar to that observed in normal tissue. These data strongly suggest that CQ has selective activity on tumor cells, where more cellular Cu is available, but has less effect on normal tissue.

Most Cu within cells is in the Cu(I) state [Pufahl et al., 1997; Ohgami et al., 2006]. Previous Cu XANES studies [Yang et al., 2005] on mouse NIH 3T3 cells revealed a predominant Cu(I) species in all cell regions studied. Although our samples were fixed in formaldehyde and the NIH 3T3 cells were fixed in methanol/acetone, current XANES results reflect similar spectral features. This could be explained by the fact that Cu uptake by cells is controlled by the Cu transporter Ctr1 [Harris, 2000]. Ctr1 located on the cell membrane recognizes only the reduced form of Cu. Therefore, in order to be transported into the cells by Ctr1, Cu(II) has to be reduced to Cu(I) first before entering a cell [Ohgami et al., 2006; Chen and Dou,

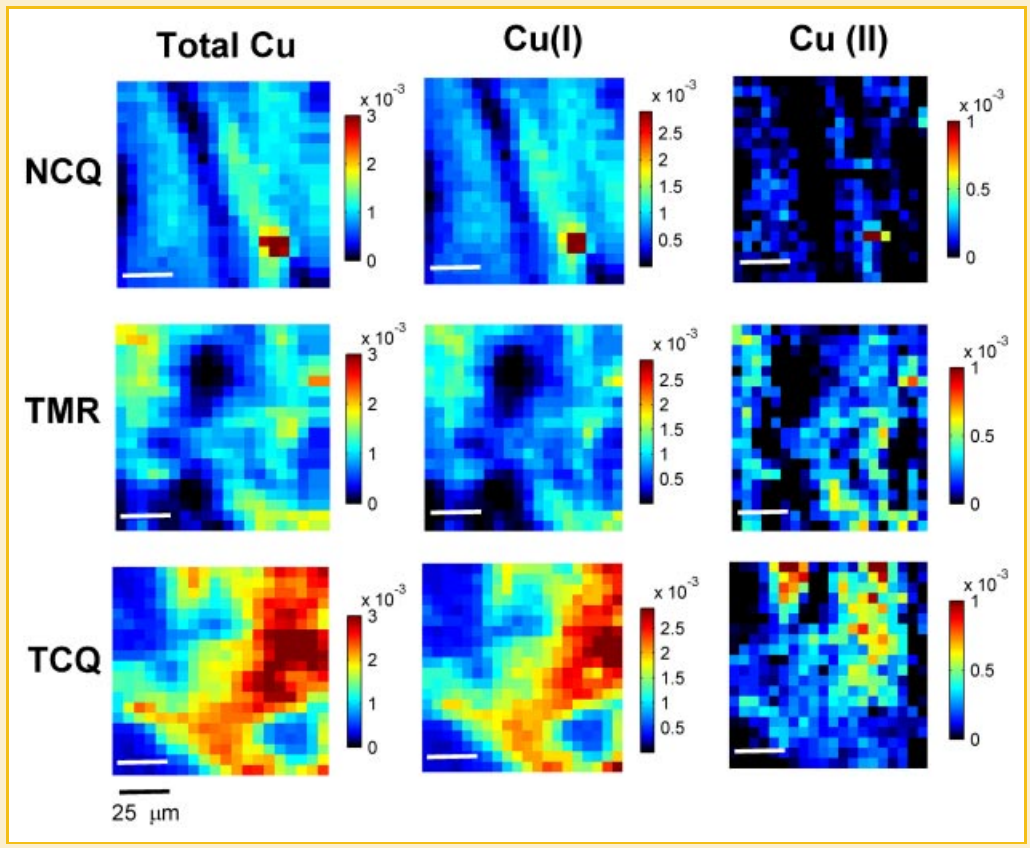

Fig. 5. Total Cu, Cu(I), and Cu(II) content in normal and tumor tissue by XFM is shown. The speciation-map images show the spatial distribution of total Cu content as compared to the corresponding Cu(I) and Cu(II) content per pixel. The intensity scale shown at the right side of each map represents the relative intensities of each Cu species. See Materials and Methods Section for details.

2008]. Within a cell, Cu is bound to various chaperones that are reducing proteins and would keep intracellular Cu as Cu(I) [Pufahl et al., 1997]. No direct evidence for the presence of Cu(II) in normal tissue was available although the presence of small amounts locally of this Cu species cannot be completely discounted. In contrast, we show unequivocal evidence for the presence of Cu(II) in tumor cells. It has been documented that CQ is a Cu chelator and the theoretical binding energies of CQ–Cu is 685.26 (kcal/mol) [Ji and Zhang, 2005]. We have been unable to find literature data concerning the electronic affinity of cellular chaperones for Cu but we assume that CQ could chelate at least some of the Cu in a cell and serum from Cu chaperone proteins.

Importantly, we found that CQ treatment increased the Cu(II)/Cu(I) ratio in tumors, compared with the Cu(II)/Cu(I) ratio observed in the untreated tumors (Fig. 5). This could be interpreted by: (i) CQ has a stronger affinity for Cu than some of the Cu chaperone proteins in the cell and binds and oxidizes Cu forming a CQ–Cu(II) complex; (ii) CQ selectively reacts with Cu(II) in tumor but not normal tissue, forming a CQ–Cu(II) complex; (iii) CQ may bind to a exogenous Cu and forms a CQ–Cu(II) complex then transported into tumor cells. This finding indicates that Cu(II) in a tumor cell may be the "killing" form of Cu (presented as a CQ–Cu(II) complex in this study) to induce apoptotic cell death and inhibit proteasome activity.

CONCLUSIONS

In summary, our studies show that (i) the increase of Cu content in tumor tissue is accompanied by an increased Cu/Zn ratio; (ii) Cu/Zn balances in tumor, but not normal, tissue change significantly after treatment with CQ; (iii) CQ treatment also increases the ratio of Cu(II)/Cu(I) in tumor but not normal tissue although Cu(I) is predominant in both normal and tumor tissues; (iv) CQ-induced Cu(II) may be the active form of CQ–Cu complex that inhibits proteasome activity and induces apoptosis in CQ-treated human tumor xenografts. This study strongly suggests that CQ has selective activity on tumor cells, where more cellular Cu is available, and has little effect on normal tissue.

MATERIALS AND METHODS

XENOGRAFT EXPERIMENTS

Male athymic nude mice (5-week-old, Taconic Research Animal Services (Hudson, NY) were used in our in vivo experiments. Briefly, human prostate cancer C4-2B cells (5×10^6) were injected subcutaneously (s.c.) into one flank of each mouse. When the tumor size reached 200 mm^3, the mice were divided into two groups

(n = 8) and treated with either solvent (mixture of cremophor/PBS/ethanol/DMSO = 5:2:2:1) or Clioquinol (10 mg/kg/day). Tumors and normal tissues from mouse flank were collected after 15-day treatment for related analysis. Tumor samples were obtained from the human prostate tumor C4-2B xenografts grown in nude mice, while the normal tissues were from the sites adjacent to the xenografts form the same mice. In addition, aliquots of the tissue samples were verified to be tumor and normal tissues by anatomy and H&E staining analysis. From each piece of tissue at least three samples were prepared for analysis.

TISSUE SAMPLES

Thin sections of both tumor and adjacent normal tissue samples were prepared as follows. Tissues were washed and stored in 10% sucrose solution (prepared with nano-pure water to prevent any external metal contamination) at 4°C for 24 h. After soaking, tissues were snap frozen in liquid nitrogen and stored at −70°C. Samples were then fixed in 4% formaldehyde for 24 h. Cryosections of the tissues were cut with a Tissue Tek machine at a thickness of 10 μ and deposited on a custom designed sample holder consisting of a 1 mm thick acrylic plate with a 10 mm × 10 mm square hole. The square hole is covered with an 8 μ Kapton film. The following four groups of samples were prepared for the microprobe experiment: (a) tumor sections of mice from control group (TMR); (b) adjacent normal tissue sections of mice from control group (NCON); (c) tumor sections of mice from CQ-treated group (TCQ); (d) adjacent normal tissue of mice from CQ-treated group (NCQ).

Cu STANDARDS FOR MICROPROBE AND SPECIATION MEASUREMENTS

$Cu(II)Cl_2$, $Cu(II)SO_4$, Cu(II)O, and $Cu_2(I)O$ samples used as Cu(I) and Cu(II) references were purchased from Sigma–Aldrich (St. Louis, MO); Standard Reference Material 1566b Oyster Tissue used as Fe, Cu, and Zn content reference was purchased from NIST (Gaithersburg, MD). The oyster tissue standard was prepared following NIST recommendations to ensure accuracy.

X-RAY FLUORESCENCE MICROPROBE

The distribution and concentration of trace elements in prostate tissue samples were measured with X-ray fluorescence microprobe. The experiments were carried out at the Biophysics Collaborative Access Team (BioCAT) undulator beamline 18ID at the Advanced Photon Source, Argonne National Laboratory. The undulator X-ray beam was tuned to 10 keV by using the beamline cryo-cooled monochromator #1 [Fischetti et al., 2004]. An XRADIA KB mirror system focused the X-ray beam down to a 5 μm × 5 μm Full Width at Half Maximum (FWHM) focal spot with a delivered intensity of ca. 3×10^{11} photons/s, measured using an ion chamber downstream of the mirrors [Barrea et al., 2006]. The signal from each 25 μm^2 pixel represents the average elemental content of either a whole cell or a group of cells (since subcellular compartments would not be resolved at this resolution). Areas of tissue sections 200 μm × 500 μm were scanned to produce each image (>4,000 pixels). The florescence signal was collected with a 100 mm^2 active area Ketek silicon drift detector (SDD). The samples and SDD detector were located 45° and 90° relative to the incoming beam direction, respectively. The data was collected by scanning the sample across the beam in a series of steps using BioCAT's software routine "FMap" at a rate of 1.0 s/pixel. More details of the microprobe experimental setup can be found elsewhere [Barrea et al., 2006].

X-RAY ABSORPTION SPECTROSCOPY

Bulk XANES experiment at the Cu K absorption edge (8,979 eV) was performed to identify the species of Cu present on NCON, TMR, and TCQ samples. The incoming X-ray beam was unfocused and collimated to 0.5 mm × 0.5 mm (FWHM) with the rest of the setup being the same as the fluorescence microprobe experiment. The X-ray beam was scanned over a selected energy range around the Cu K absorption edge in continuous scanning mode (scan time: 30 s) [Barrea et al., 2005]. The low signal to noise ratio of the measured spectra is mainly caused by the very low Cu content in both normal and tumor tissue samples. Scans were repeated several times to obtain adequate counting statistics (10 times in case of the Cu standards and 100 times in case of the tissue samples). Different sample spots were exposed to the beam by rastering the samples in the XY direction minimizing this way the exposure time of a given sample spot to avoid radiation damage effects. Both Cu standards and tissue samples were measured under the same experimental conditions. XANES spectra of Cu standards are shown in Figure 4. Cu(II) species (CuO, $CuCl_2$, and $CuSO_4$ standards) show a very weak pre-edge peak ($1s \rightarrow 3d$ transition) at 8,978 eV (line a). This peak is completely absent in Cu(I) samples (Cu_2O standard). The sharp pre-edge peak at 8,983 eV is only observed in Cu(I) samples and it represents a $1s \rightarrow 4d$ transition (Fig. 4 line b). The intensity of this transition varies with Cu(I) geometry (ca. 0.6 normalized intensity in tetrahedral geometry up to ca. 1.0 normalized intensity in two-coordinated linear geometry [Kau et al., 1987; Yang et al., 2005]. Cu(II) species show a very weak tail at this energy (0.1–0.2 normalized intensity). A very intense shoulder around 8,987–8,989 eV is observed in Cu(II) samples (Fig. 4 line c); its intensity and location depends on the Cu ligands: S, Cl, N, or O. A prominent shoulder at 8,995 eV is also observed in Cu(I) samples (Fig. 4, line d). The spectral intensity at 9,080 eV (not shown in Fig. 4) is independent of the Cu chemical speciation status and is used for normalization purposes.

X-RAY FLUORESCENCE SPECIATION MAPPING

To identify the chemical status of Cu locally, we performed X-ray microfluorescence Cu speciation mapping on each of the NCQ, TMR, and TCQ samples using a two excitation energy approach [Pickering et al., 2000]. Two Cu Kα fluorescence maps, at excitation energies E1 = 8,983 eV and E2 = 9,080 eV, were measured for each tissue sample. These energies were selected considering the spectral features observed in bulk measurements: 8,983 eV (Fig. 4, line b) where Cu(I) pre-edge peak is observed, and 9,080 eV (not shown in the picture) as normalization value. The measured fluorescence maps were analyzed using the following relationships: Cu(I) normalized intensity = 0.7 and 1.0 at E1 and E2, respectively (assuming a trigonal bonding geometry) and Cu(II) normalized intensity = 0.1 and 1.0 at E1 and E2, respectively. We assumed the measured intensity was a linear combination of both Cu(I) and Cu(II)

intensities in order to obtain the partial concentration of each species. The acquisition time per pixel was 10 s at each energy.

ACKNOWLEDGMENTS

This work was supported by Karmanos Cancer Institute of Wayne State University, Department of Defense Breast Cancer Research Program awards W81XWH-04-1-0688 and DAMD17-03-1-0175, and National Cancer Institute grant CA112625 (Q. P. Dou) and the National Cancer Institute/NIH Cancer Center Support grant (Karmanos Cancer Institute). The Biophysics Collaborative Access Team is a NIH-supported research center, RR08630. Use of the Advanced Photon Source was supported by the U.S. Department of Energy, Basic Energy Science, Office of Energy Research, under contract no. W-31-109-Eng-38. The content is solely the responsibility of the authors and does not necessarily reflect the official views of the National Center for Research Resources or the National Institutes of Health.

REFERENCES

Amici M, Forti K, Nobili C, Lupidi G, Angeletti M, Fioretti E, Eleuteri AM. 2002. Effect of neurotoxic metal ions on the proteolytic activities of the 20S proteasome from bovine brain. J Biol Inorg Chem 7:750–756.

Barrea RA, Fischetti R, Stepanov S, Rosenbaum G, Kondrashkina E, Bunker GB, Black E, Zhang K, Gore D, Heurich R, Vukonich M, Karanfil C, Kropf AJ, Wang S, Irving TC. 2005. Biological XAFS at the BioCAT Undulator Beamline 18ID at the APS. Phys Scripta T115:867–869.

Barrea RA, Gore D, Kondrashkina E, Weng T, Heurich R, Vukonich M, Orgel J, Davidson M, Collingwood JF, Mikhaylova A, Irving TC. 2006. The BioCAT Microprobe for X-ray Fluorescence Imaging, MicroXAFS and Microdiffraction Studies on Biological Samples. In: Proc 8th Int Conf X-ray Microscopy IPAP Conf Series 7; pp 230–232.

Brem S. 1999. Angiogenesis and cancer control: From concept to therapeutic trial. Cancer Control 6:436–458.

Brewer GJ. 2001. Copper control as an antiangiogenic anticancer therapy: Lessons from treating Wilson's disease. Exp Biol Med (Maywood) 226:665–673.

Brewer GJ, Dick RD, Grover DK, LeClaire V, Tseng M, Wicha M, Pienta K, Redman BG, Jahan T, Sondak VK, Strawderman M, LeCarpentier G, Merajver SD. 2000. Treatment of metastatic cancer with tetrathiomolybdate, an anticopper, antiangiogenic agent: Phase I study. Clin Cancer Res 6:1–10.

Chen D, Dou QP. 2008. New uses for old copper-binding drugs: Converting the pro-angiogenic copper to a specific cancer cell death inducer. Expert Opin Ther Targets 12:739–748.

Chen D, Peng F, Cui QC, Daniel KG, Orlu S, Liu J, Dou QP. 2005. Inhibition of prostate cancer cellular proteasome activity by a pyrrolidine dithiocarbamate-copper complex is associated with suppression of proliferation and induction of apoptosis. Front Biosci 10:2932–2939.

Chen D, Cui QC, Yang H, Barrea RA, Sarkar FH, Sheng S, Yan B, Reddy GP, Dou QP. 2007. Clioquinol, a therapeutic agent for Alzheimer's disease, has proteasome-inhibitory, androgen receptor-suppressing, apoptosis-inducing, and antitumor activities in human prostate cancer cells and xenografts. Cancer Res 67:1636–1644.

Costello LC, Franklin RB. 1998. Novel role of zinc in the regulation of prostate citrate metabolism and its implications in prostate cancer. Prostate 35:285–296.

Daniel KG, Gupta P, Harbach RH, Guida WC, Dou QP. 2004. Organic copper complexes as a new class of proteasome inhibitors and apoptosis inducers in human cancer cells. Biochem Pharmacol 67:1139–1151.

Daniel KG, Chen D, Orlu S, Cui QC, Miller FR, Dou QP. 2005. Clioquinol and pyrrolidine dithiocarbamate complex with copper to form proteasome inhibitors and apoptosis inducers in human breast cancer cells. Breast Cancer Res 7:R897–R908.

Degen PH, Moppert J, Schmid K, Weirich EG. 1979a. Percutaneous absorption of chlorquinaldol (Sterosan). Dermatologica 159:239–244.

Degen PH, Moppert J, Schmid K, Weirich EG. 1979b. Percutaneous absorption of clioquinol (Vioform). Dermatologica 159:295–301.

Di Vaira MBC, Orioli P, Messori L, Bruni B, Zatta P. 2004. Clioquinol, a drug for Alzheimer's disease specifically interfering with brain metal metabolism: Structural characterization of its zinc(II) and copper(II) complexes. Inorg Chem 43:3795–3797.

Ferrada E, Arancibia V, Loeb B, Norambuena E, Olea-Azar C, Huidobro-Toro JP. 2007. Stoichiometry and conditional stability constants of Cu(II) or Zn(II) clioquinol complexes; implications for Alzheimer's and Huntington's disease therapy. Neurotoxicology 28:445–449.

Finney L, Mandava S, Ursos L, Zhang W, Rodi D, Vogt S, Legnini D, Maser J, Ikpatt F, Olopade OI, Glesne D. 2007. X-ray fluorescence microscopy reveals large-scale relocalization and extracellular translocation of cellular copper during angiogenesis. Proc Natl Acad Sci USA 104:2247–2252.

Fischetti R, Stepanov S, Rosenbaum G, Barrea R, Black E, Gore D, Heurich R, Kondrashkina E, Kropf AJ, Wang S, Zhang K, Irving TC, Bunker GB. 2004. The BioCAT undulator beamline 18ID: A facility for biological noncrystalline diffraction and X-ray absorption spectroscopy at the Advanced Photon Source. J Synchrotron Rad 11:399–405.

Goodman VL, Brewer GJ, Merajver SD. 2004. Copper deficiency as an anticancer strategy. Endocr Relat Cancer 11:255–263.

Guntupalli JN, Padala S, Gummuluri AV, Muktineni RK, Byreddy SR, Sreerama L, Kedarisetti PC, Angalakuduru DP, Satti BR, Venkatathri V, Pullela VB, Gavarasana S. 2007. Trace elemental analysis of normal, benign hypertrophic and cancerous tissues of the prostate gland using the particle-induced X-ray emission technique. Eur J Cancer Prev 16:108–115.

Gupta SK, Shukla VK, Vaidya MP, Roy SK, Gupta S. 1991. Serum trace elements and Cu/Zn ratio in breast cancer patients. J Surg Oncol 46:178–181.

Habib FK, Mason MK, Smith PH, Stitch SR. 1979. Cancer of the prostate: Early diagnosis by zinc and hormone analysis? Br J Cancer 39:700–704.

Habib FK, Dembinski TC, Stitch SR. 1980. The zinc and copper content of blood leucocytes and plasma from patients with benign and malignant prostates. Clin Chim Acta 104:329–335.

Harris ED. 2000. Cellular copper transport and metabolism. Annu Rev Nutr 20:291–310.

Huang YL, Sheu JY, Lin TH. 1999. Association between oxidative stress and changes of trace elements in patients with breast cancer. Clin Biochem 32: 131–136.

Ide-Ektessabi AFS, Sugimura K, Kitamura Y, Gotoh A. 2002. Quantitative analysis of zinc in prostate cancer tissues using synchrotron radiation microbeams. X-Ray Spectrom 31:7–11.

Inutsuka S, Araki S. 1978. Plasma copper and zinc levels in patients with malignant tumors of digestive organs: Clinical evaluation of the C1/Zn ratio. Cancer 42:626–631.

Jemal A, Siegel R, Ward E, Murray T, Xu J, Smigal C, Thun MJ. 2006. Cancer statistics, 2006. CA Cancer J Clin 56:106–130.

Ji HF, Zhang HY. 2005. A new strategy to combat Alzheimer's disease. Combining radical-scavenging potential with metal-protein-attenuating ability in one molecule. Bioorg Med Chem Lett 15:21–24.

Kau LS-SD, Penner-Hahn J, Hodgson K, Solomon E. 1987. X-Ray absorption edge determination of the oxidation state and coordination number of copper. Application to the type 3 site in Rhus vernicifera laccase and its reaction with oxygen. J Am Chem Soc 109:6433–6442.

Kim I, Kim CH, Kim JH, Lee J, Choi JJ, Chen ZA, Lee MG, Chung KC, Hsu CY, Ahn YS. 2004. Pyrrolidine dithiocarbamate and zinc inhibit proteasome-dependent proteolysis. Exp Cell Res 298:229–238.

Lightman A, Brandes JM, Binur N, Drugan A, Zinder O. 1986. Use of the serum copper/zinc ratio in the differential diagnosis of ovarian malignancy. Clin Chem 32:101–103.

Macreadie IG. 2008. Copper transport and Alzheimer's disease. Eur Biophys J 37:295–300.

Milacic V, Chen D, Giovagnini L, Diez A, Fregona D, Dou QP. 2008. Pyrrolidine dithiocarbamate-zinc(II) and -copper(II) complexes induce apoptosis in tumor cells by inhibiting the proteasomal activity. Toxicol Appl Pharmacol 231:24–33.

Nayak SB, Bhat VR, Upadhyay D, Udupa SL. 2003. Copper and ceruloplasmin status in serum of prostate and colon cancer patients. Indian J Physiol Pharmacol 47:108–110.

Nguyen T, Hamby A, Massa SM. 2005. Clioquinol down-regulates mutant huntingtin expression in vitro and mitigates pathology in a Huntington's disease mouse model. Proc Natl Acad Sci USA 102:11840–11845.

Nitzan YB, Sekler I, Frederickson CJ, Coulter DA, Balaji RV, Liang SL, Margulis A, Hershfinkel M, Silverman WF. 2003. Clioquinol effects on tissue chelatable zinc in mice. J Mol Med 81:637–644.

Ohgami RS, Campagna DR, McDonald A, Fleming MD. 2006. The Steap proteins are metalloreductases. Blood 108:1388–1394.

Parke A, Bhattacherjee P, Palmer RM, Lazarus NR. 1988. Characterization and quantification of copper sulfate-induced vascularization of the rabbit cornea. Am J Pathol 130:173–178.

Pickering IJ, Prince RC, Salt DE, George GN. 2000. Quantitative, chemically specific imaging of selenium transformation in plants. Proc Natl Acad Sci USA 97:10717–10722.

Pufahl RA, Singer CP, Peariso KL, Lin SJ, Schmidt PJ, Fahrni CJ, Culotta VC, Penner-Hahn JE, O'Halloran TV. 1997. Metal ion chaperone function of the soluble Cu(I) receptor Atx1. Science 278:853–856.

Puig S, Thiele DJ. 2002. Molecular mechanisms of copper uptake and distribution. Curr Opin Chem Biol 6:171–180.

Rae TD, Schmidt PJ, Pufahl RA, Culotta VC, O'Halloran TV. 1999. Undetectable intracellular free copper: The requirement of a copper chaperone for superoxide dismutase. Science 284:805–808.

Raju KS, Alessandri G, Ziche M, Gullino PM. 1982. Ceruloplasmin, copper ions, and angiogenesis. J Natl Cancer Inst 69:1183–1188.

Ritchie CW, Bush AI, Mackinnon A, Macfarlane S, Mastwyk M, MacGregor L, Kiers L, Cherny R, Li QX, Tammer A, Carrington D, Mavros C, Volitakis I, Xilinas M, Ames D, Davis S, Beyreuther K, Tanzi RE, Masters CL. 2003. Metal-protein attenuation with iodochlorhydroxyquin (clioquinol) targeting Abeta amyloid deposition and toxicity in Alzheimer disease: A pilot phase 2 clinical trial. Arch Neurol 60:1685–1691.

Ritchie CW, Bush AI, Masters CL. 2004. Metal-protein attenuating compounds and Alzheimer's disease. Expert Opin Investig Drugs 13:1585–1592.

Rizk SL, Sky-Peck HH. 1984. Comparison between concentrations of trace elements in normal and neoplastic human breast tissue. Cancer Res 44:5390–5394.

Theophanides T, Anastassopoulou J. 2002. Copper and carcinogenesis. Crit Rev Oncol Hematol 42:57–64.

Turecky L, Kalina P, Uhlikova E, Namerova S, Krizko J. 1984. Serum ceruloplasmin and copper levels in patients with primary brain tumors. Klin Wochenschr 62:187–189.

Vallee BL, Auld DS. 1990. Active-site zinc ligands and activated H2O of zinc enzymes. Proc Natl Acad Sci USA 87:220–224.

Yang L, McRae R, Henary MM, Patel R, Lai B, Vogt S, Fahrni CJ. 2005. Imaging of the intracellular topography of copper with a fluorescent sensor and by synchrotron x-ray fluorescence microscopy. Proc Natl Acad Sci USA 102:11179–11184.

Zaichick V, Sviridova TV, Zaichick SV. 1997. Zinc in the human prostate gland: Normal, hyperplastic and cancerous. Int Urol Nephrol 29:565–574.